PNAS RESEARCH ARTICLE | NEUROSCIENCE

Dopamine D1 and D2 receptors differentially control strength and dynamics of abstract decision codes in the primate prefrontal cortex

Esther F. Kutter[a,1], Pooja Viswanathan[a,1], and Andreas Nieder[a,2]

Affiliations are included on p. 10.

Edited by Ranulfo Romo, El Colegio Nacional, Mexico City, DF, Mexico; received January 4, 2026; accepted March 13, 2026

Dopamine critically modulates prefrontal circuits underlying cognitive control, but how D1-type (D1R) and D2-type (D2R) receptors influence abstract decision coding is unclear. We recorded single-neuron activity in two monkeys performing a number comparison task, in which abstract decisions about sequentially presented dot displays were dissociated from motor responses, while locally stimulating D1R or D2R via microiontophoresis. D1R stimulation suppressed, whereas D2R stimulation enhanced, the decision-coding strength of individual neurons, effects mirrored at the population level in decoding accuracy. Interestingly, dopamine receptors also bidirectionally modulated the temporal structure of population activity: D1R stimulation reduced the temporal generalizability of neuronal decision selectivity, suggesting more transient tuning and a shift toward a more dynamic coding regime. Conversely, D2R stimulation increased temporal generalizability of decision selectivity, implying more sustained tuning and a shift toward a more static coding regime. These findings suggest that D1- and D2-mediated mechanisms in the prefrontal cortex provide a receptor-specific substrate for balancing cognitive flexibility and stability in abstract decision-making. This pattern may reflect task-dependent deviations from classical dual-state models, in which D1 receptor activity stabilizes working memory representations whereas D2 receptor activity supports flexible coding—a relationship that appears reversed in the context of abstract decision formation.

primate prefrontal cortex | decision-making | dopamine | coding dynamics

Significance

How dopamine shapes abstract decision-making in the prefrontal cortex remains a central unresolved problem in neuroscience. Using causal, receptor-specific manipulations combined with single-neuron recordings in behaving primates, we show that D1 and D2 dopamine receptors exert opposing and highly precise control over both the strength and temporal organization of prefrontal decision representations. D1 receptors suppress and destabilize decision codes, promoting dynamic, transient population activity, whereas D2 receptors enhance and stabilize sustained, attractor-like representations. These findings revise the classic dual-state theory of prefrontal dopamine by revealing receptor-specific control over the temporal architecture of abstract cognition, providing a mechanistic link between dopamine signaling, cognitive flexibility, and stability.

The prefrontal cortex (PFC) orchestrates cognitive control by selecting relevant information, maintaining it in working memory, and applying behavioral rules (1, 2). Decision-making exemplifies this control, enabling judgments among alternatives based on available information. In traditional models of decision-making, choices are often conflated with action plans, implying that cortical decision signals primarily reflect motor preparation rather than abstract evaluation (3–5). However, decisions can also manifest as action-independent cognitive states—abstract decisions—that encode categorical judgments detached from immediate motor demands (6–12).

To enable abstract decisions, the brain requires a working-memory buffer that transiently bridges sensory input and forthcoming motor output. The neuronal foundation of working memory lies in the selective activity of PFC neurons that encode task-relevant information across delay periods (13, 14). Traditionally, working memory has been conceptualized as sustained, selective neural activity that persists throughout the delay period, maintaining a stable and static code to bridge temporal gaps between perception and action (13, 15–18). However, emerging evidence indicates that working memory often relies on dynamic population codes, where neurons with mixed and time-varying selectivity collectively sustain information (19–22). Given this flexibility in neural coding, it is plausible that PFC neurons can adjust the relative contribution of static and dynamic activity under neuromodulatory influence. Understanding how these mechanisms regulate both the strength and temporal dynamics of abstract decision signals derived from working memory remains a central question in systems neuroscience.

Among neuromodulators, dopamine plays a central role in regulating cortical network dynamics and supporting PFC-dependent cognitive control (23–29). Dopamine, released in the PFC from midbrain neurons, acts via two primary receptor families—D1-type (D1R) with subtypes D_1 and D_5, and D2-type (D2R) with subtypes D_2, D_3, and D_4—which often exert complementary effects on neuronal coding. In the primate PFC, D1 receptors (D1Rs) are expressed across all cortical layers and are approximately 10-fold more abundant than D2 receptors (D2Rs) (30). In contrast, D2Rs show comparatively

Author contributions: P.V. and A.N. designed research; P.V. and A.N. performed research; E.F.K. and A.N. analyzed data; and E.F.K., P.V., and A.N. wrote the paper.

The authors declare no competing interest.

This article is a PNAS Direct Submission.

[1]E.F.K. and P.V. contributed equally to this work.

[2]To whom correspondence may be addressed. Email: andreas.nieder@uni-tuebingen.de.

This article contains supporting information online at https://www.pnas.org/lookup/suppl/doi:10.1073/pnas.2600210123/-/DCSupplemental.

Published April 8, 2026.

low expression in most layers, with highest densities observed in layer V (31, 32). Both receptor types are present on pyramidal neurons as well as inhibitory interneurons, indicating that dopamine can modulate excitatory and inhibitory circuits via both D1- and D2-mediated mechanisms (33–35).

D1 receptors (D1Rs) enhance the stability and maintenance of task-relevant information by boosting signal-to-noise ratios and strengthening recurrent excitation in prefrontal networks, thereby supporting selective activity and resistance to distraction (23, 36–40). In contrast, D2 receptors (D2Rs) promote cognitive flexibility by enhancing neuronal excitability and supporting dynamic network states that facilitate the updating and switching of working memory representations (29, 41–44). Together, D1R- and D2R-mediated mechanisms enable dopamine to balance the competing demands of cognitive stability and flexibility, a fundamental feature of adaptive prefrontal function (26, 45). Computational models formalize this dichotomy in the "dual-state theory" of prefrontal dopamine function, proposing that D1R and D2R activation bias cortical networks toward stable or flexible states, respectively (25, 29, 36). Within this framework, a D1R-dominated state stabilizes attractor networks, enhancing persistent activity and shielding working memory representations from interference. Conversely, a D2R-dominated state reduces attractor barriers, promoting flexible switching between representations and enabling rapid updating of working memory content. Despite its explanatory power, direct neurophysiological evidence for how D1R and D2R activation shapes the temporal dynamics of abstract decision coding remains limited.

To address this gap, we investigated rhesus macaque monkeys, which exhibit well-established numerical competence and abstract quantity representations (46, 47). We trained monkeys on a numerical comparison task designed to dissociate abstract "same/different" decisions from both their sensory inputs and motor outputs (11). We then combined single-neuron recordings in the dorsolateral PFC (dlPFC), a brain area known to contain number-selective neurons (48–51), with the microiontophoretic application of a D1R or D2R agonist. This approach allowed us to test two key hypotheses: First, that D1R and D2R stimulation would modulate the decision-coding strength of single neurons, and that these effects would be opposing. If so, these effects would be evident in the population's ability to decode abstract decisions; second, that dopamine receptor manipulation would bidirectionally alter the temporal format of the population code, shifting it between a stable, persistent state and a more dynamic, transient one. Our results confirm these hypotheses, providing a mechanistic link between dopamine receptor function and the dynamic neural codes that underlie abstract thought.

Results

We trained two monkeys to compare the numerosities of sequentially presented dot displays and indicate whether they were the same or different (11). The displays contained 1, 3, or 9 dots, with low-level visual features controlled for their covariation with numerosity (Fig. 1*A*). To ensure that the monkeys based their judgments on numerical rather than nonnumerical stimulus properties, we applied two stimulus protocols. In the "standard" condition, dot radii and interdot distances varied randomly, whereas in the "control" condition, total dot area and interdot distance were held constant across numerosities.

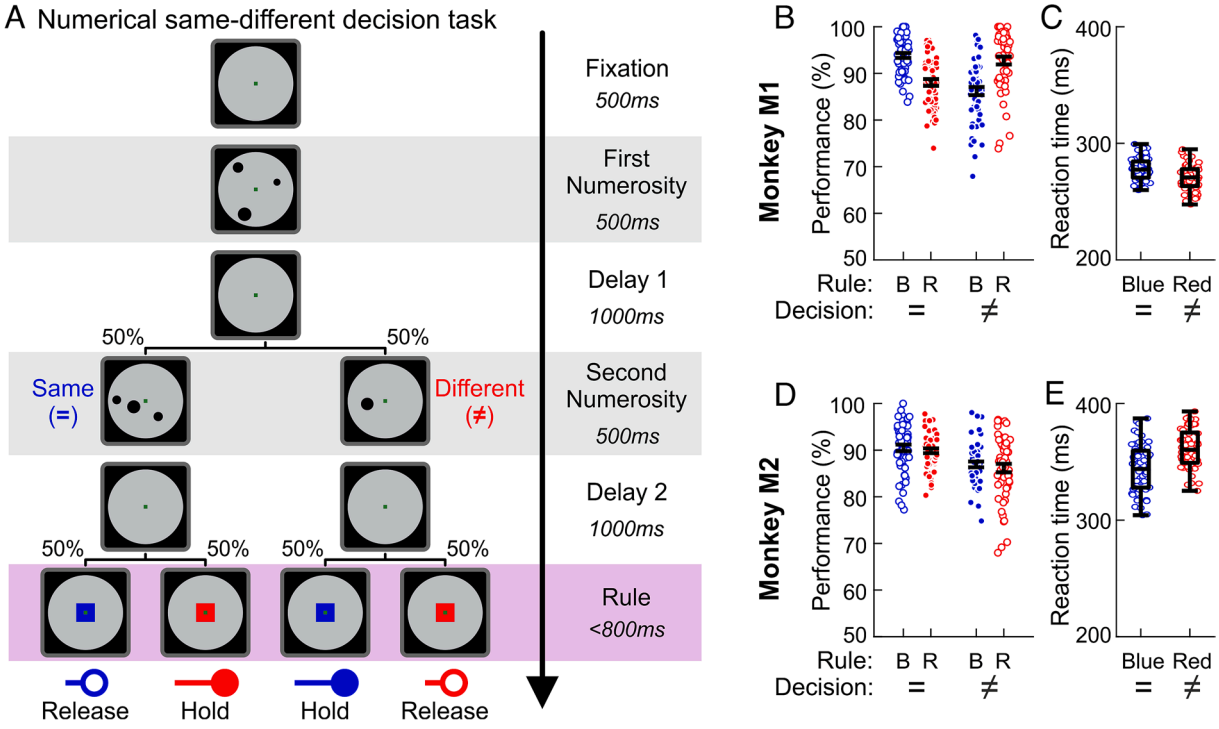

Fig. 1. Numerical decision task and behavior. (*A*) Experimental task. After an initial fixation period, two dot displays were shown in sequence, interspersed by a delay of 1,000 ms, respectively. During the subsequent presentation of a rule cue period, the monkey responded by either releasing a response bar held throughout the trial or by maintaining the hold. The *Left* column shows the task contingencies for "same" numerosities, the *Right* column for "different" numerosities (50% of the trials each). Only correct combinations of decisions and motor rules (orthogonalized for the two decisions) were rewarded by fluid. (*B*) Behavioral performance for monkey M1, split by rule cues (B, blue; R, red) for each decision. Individual circles depict behavioral sessions; filled circles corresponding to "hold" motor responses, and empty circles corresponding to "release" responses. Black bars show the mean ± SEM. (*C*) Reaction times for monkey M1 during trials that correctly required a bar release, determined as time from rule cue onset to monkey's release. Individual circles depict behavioral sessions; box plots show median with 25 to 75% CI. (*D*) Behavioral performance for monkey M2. Same conventions as in *B*. (*E*) Reaction times for monkey M2. Same conventions as in *C*.

After viewing the two displays, the monkeys made and maintained their decision during a second delay period (Delay 2) until a response rule appeared, instructing them how to indicate whether the numerosities were the same or different. Because the action plan was dissociated from the decision during Delay 2, we refer to this as an "abstract decision." If the two numerosities matched, a blue square cued bar release and a red square cued bar hold; if they differed, the rule contingencies were reversed. We systematically varied five factors (*Methods*): the numerosities of the first and second stimuli (1, 3, or 9), decision outcome (same/ different), stimulus protocol (standard/control), and rule cue (red/blue).

Behavior. Both monkeys performed well above chance (50%) across all sessions (Fig. 1 *B* and *D*), with mean accuracy around 90% across rule–decision conditions. Monkey M1 performed mildly better on bar-release than bar-hold trials (ΔPerformance = 6.2% ± 0.8%; P_{IA} = 1.8953 × 10^{-14}; 2-way ANOVA with factors rule cue × decision; n = 57 sessions; Fig. 1*B*), whereas monkey M2 showed slightly higher accuracy for "same" compared to "different" decisions (ΔPerformance = 3.6% ± 0.6%; P_{Dec} = 5.0734 × 10^{-7}; n = 57 sessions; Fig. 1*D*).

In trials requiring an immediate bar release, we also measured reaction times (RTs), defined as the interval from rule-cue onset to bar release. For both monkeys, RTs differed significantly across rule–decision combinations (Fig. 1 *C* and *E*). Monkey M1 responded slightly faster in "red + different" than "blue + same" trials (ΔRT = 6.6 ms ± 1.4 ms; P = 0.0006194, Z = –3.423; two-sided Wilcoxon rank sum test; n = 57 sessions; Fig. 1*C*), whereas monkey M2 showed the opposite pattern (ΔRT = –16.5 ms ± 2.5 ms; P = 4.3878 × 10^{-5}, Z = 4.0861; n = 57 sessions; Fig. 1*E*). Together, these behavioral results demonstrate that the monkeys understood the rule cues and successfully integrated them with the preceding numerical decision.

Single Neurons Encode Decision Information Dynamically. In a previous study (11), we used this task to demonstrate that abstract numerical comparison decisions can be decoded from single neurons in primate PFC, independent of sensory and motor processes. Here, we applied microiontophoretic dopamine-drug application to investigate how dopamine D1 and D2 receptor families influence the decision-coding properties of PFC neurons.

We recorded 442 single neurons centered on the principal sulcus in the (dlPFC; M1: 166 neurons, M2: 276 neurons) across 114 sessions (57 per monkey) while the animals performed the task (Fig. 2*A*). In baseline conditions (without drug application), many dlPFC neurons selectively encoded abstract decision information during Delay 2, when numerical evidence was available but the required motor response was still unknown (Fig. 3). Some neurons increased firing for "same" decisions (Fig. 3 *A* and *C*), whereas others preferred "different" decisions (Fig. 3 *B* and *D*).

To identify selectivity to different task factors over time, we performed sliding-window linear mixed-effects (LME) regression on each neuron's responses, using "first numerosity," "second numerosity," "stimulus protocol," and "decision" as factors (evaluated at α = 0.05) (*Methods*). Neurons processed different task information sequentially (Fig. 4*A*): The population stably represented first numerosity (270/442 cells; 61%) and second numerosity (213/442 cells; 48%) during stimulus presentation and the subsequent delays. Crucially, abstract decisions were continuously represented in the population (277/442 cells; 63%) from the onset of the second numerosity until the end of Delay 2. Similar proportions of selectivity were seen in both monkeys separately (*SI Appendix*, Table S1). Many neurons exhibited dynamic tuning, showing brief, nonpersistent intervals of significant decision coding with variable onset latencies (Fig. 4*B*), and mixed selectivity for multiple factors. Nevertheless, a substantial subset (127/442 cells; 29%) was purely decision-selective, showing no significant intervals for the other three factors.

Dopamine Receptors Exert Opposite Effects on Neuronal Decision Selectivity. To directly assess the impact of dopamine receptor stimulation on abstract decision signals, we compared neuronal responses during baseline conditions (no drug) with responses recorded while microiontophoretically applying dopamine receptor agents near the recorded neurons (drug condition; *Methods*). In each session, one of two drugs was administered in drug trial blocks alternating with baseline trial blocks (Fig. 2*B*): the D1R agonist SKF81297 (n = 235 cells) or the D2R agonist quinpirole (n = 207 cells). SKF81297 is a selective agonist of D1-like dopamine receptors, activating both D1 and D5 subtypes, and is commonly used to stimulate D1-like receptor signaling. Quinpirole is a selective agonist of D2-like dopamine receptors, with high affinity for D2 and D3 subtypes, and is widely used to stimulate D2-like receptor signaling.

Consistent with previous reports (37, 43, 52, 53), D1R stimulation significantly reduced spontaneous activity during fixation (ΔFR = –0.8 Hz ± 0.3 Hz; P = 3.09 × 10^{-13}, Z = 7.291; two-sided Wilcoxon signed-rank test; n = 235 cells), whereas D2R stimulation significantly increased spontaneous activity (ΔFR = 1.3 Hz ± 0.3 Hz; P = 8.79 × 10^{-15}, Z = –7.756; n = 207 cells; Fig. 2*C*). This pattern held across all groups of numerosity-selective neurons included in the subsequent analyses (*SI Appendix*, Fig. S1).

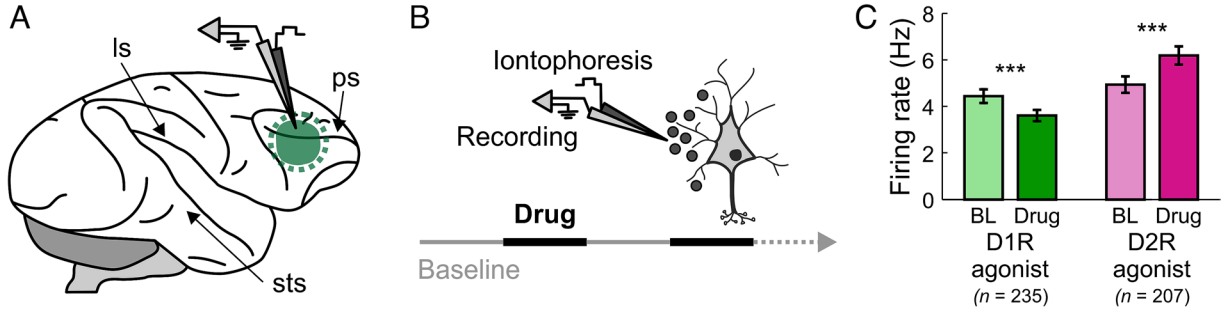

Fig. 2. Recording site and spontaneous activity. (*A*) Sagittal view of the primate brain with some anatomical landmarks (ls, lateral sulcus; ps, principal sulcus; sts, superior temporal sulcus) depicting the location of the recording site (green) in dlPFC (area 46) with simultaneous microiontophoresis. (*B*) Drug application regime. During recording, blocks of trials (n = 48) without drug application (baseline) alternate with trial blocks of drug application. Charged DA molecules are microiontophoretically applied to the extracellular vicinity of single neurons. (*C*) Effects of D1R stimulation with SKF81297 (n = 235 neurons) and D2R stimulation with quinpirole (n = 207 neurons;) on firing rates during the fixation period, compared to baseline (BL) activity without drug application. ***P < 0.001 (two-sided Wilcoxon signed-rank test); bars depict mean ± SEM.

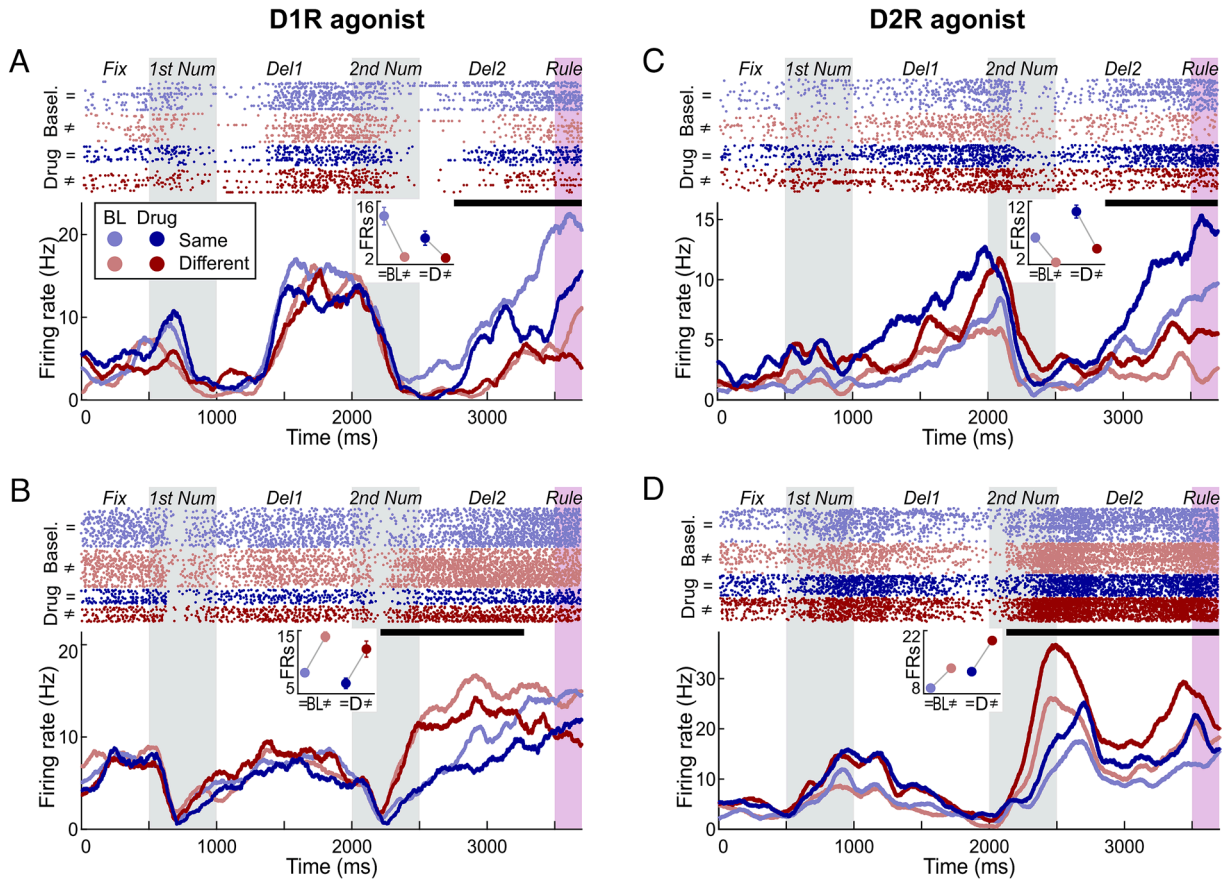

Fig. 3. Dopamine receptors (D1R and D2R) exert opposite effects on neuronal activity. (*A*) Example neuron that prefers "same" decisions during BL conditions (light colors) and after stimulating D1Rs with SKF81297 (dark colors). *Top*: Dot-raster histogram. Each row indicates one trial (color-coded per condition); each dot represents one action potential. *Bottom*: Corresponding mean instantaneous firing rates across trial time obtained by averaging responses per condition (smoothed using a 150 ms Gaussian kernel); the thickened black bar shows the significant interval in a sliding-window 4-factor LME. *Inset*: Decision tuning curves per drug condition in the selective interval; error bars denote SEM. (*B*) D1R-modulated example neuron preferring "different" decisions. Same conventions as in *A*. (*C*) Example neuron that prefers "same" conditions during BL conditions (light colors) and after stimulating D2Rs with quinpirole (dark colors). Same conventions as in *A*. (*D*) D2R-modulated example neuron preferring "different" decisions. Same conventions as in *A*.

Next, we quantified decision-coding strength of all decision neurons using the AUROC ("area under the receiver operator characteristic" derived from signal detection theory), a measure of discriminability between two distributions: 0.5 indicates no coding, whereas 1.0 indicates perfect distinction between "same" and "different" trials. We computed the AUROC for decision neurons modulated by the D1R agonist (144/235 cells; 61%) and the D2R agonist (133/207 cells; 64%) using average firing rates during intervals of significant decision coding. To assess drug effects, AUROC values were calculated separately for baseline and drug conditions (Fig. 5 and *Methods*).

In a representative neuron stimulated with the D1R agonist, decision selectivity (i.e., discriminability) during Delay 2 decreased noticeably, reflected by the smaller separation of firing rates for "same" vs. "different" decisions under the drug condition compared to baseline (*Insets* in Fig. 3 *A* and *B*). This effect was systematically observed across the population of D1R-modulated decision neurons (Fig. 5*A*): SKF81297 significantly reduced neuronal decision discriminability during intervals of significant decision coding (ΔAUROC = –0.021 ± 0.006; $P = 0.00046178$, $Z = 3.502$; two-sided Wilcoxon signed-rank test; $n = 144$ cells; Fig. 5*B*).

In contrast, D2R stimulation produced the opposite effect. A representative neuron showed increased decision selectivity under the D2R agonist, evident from the greater separation of firing rates for "same" vs. "different" decisions compared to baseline (*Insets* in Fig. 3 *C* and *D*). This effect was consistently observed across the population of D2R-modulated decision neurons (Fig. 5*C*): quinpirole significantly enhanced signal discriminability during intervals of significant decision coding (ΔAUROC = 0.024 ± 0.007; $P = 9.6257 \times 10^{-5}$, $Z = -3.8998$; $n = 133$ cells; Fig. 5*D*).

As a control to exclude influences from other task factors, we repeated the AUROC analysis using only pure decision neurons (D1R: 64/235 cells; 27%, and D2R: 63/207 cells; 21%). Even under these stringent criteria, modulation remained significant: D1R stimulation reduced decision-coding strength (ΔAUROC = –0.019 ± 0.008; $P = 0.022981$, $Z = 2.2738$; $n = 64$ cells), whereas D2R stimulation enhanced it (ΔAUROC = 0.028 ± 0.009; $P = 0.0020648$, $Z = -3.0807$; $n = 63$ cells).

Dopamine Receptor Stimulation Bidirectionally Modulates Population Decision Decoding. Single-neuron analyses revealed opposing effects of D1R and D2R stimulation on abstract decision-coding strength. We next asked whether drug application similarly modulated the population-level capacity to represent this information. To this end, we trained linear classifiers to discriminate "same" vs. "different" trials using population firing rates across time, separately for D1R-modulated ($n = 126$) and D2R-modulated ($n = 117$) neurons, and for baseline vs. drug conditions. Decoders were then tested on novel data from the same neurons to assess how well the population could predict decisions based on the training data (*Methods*).

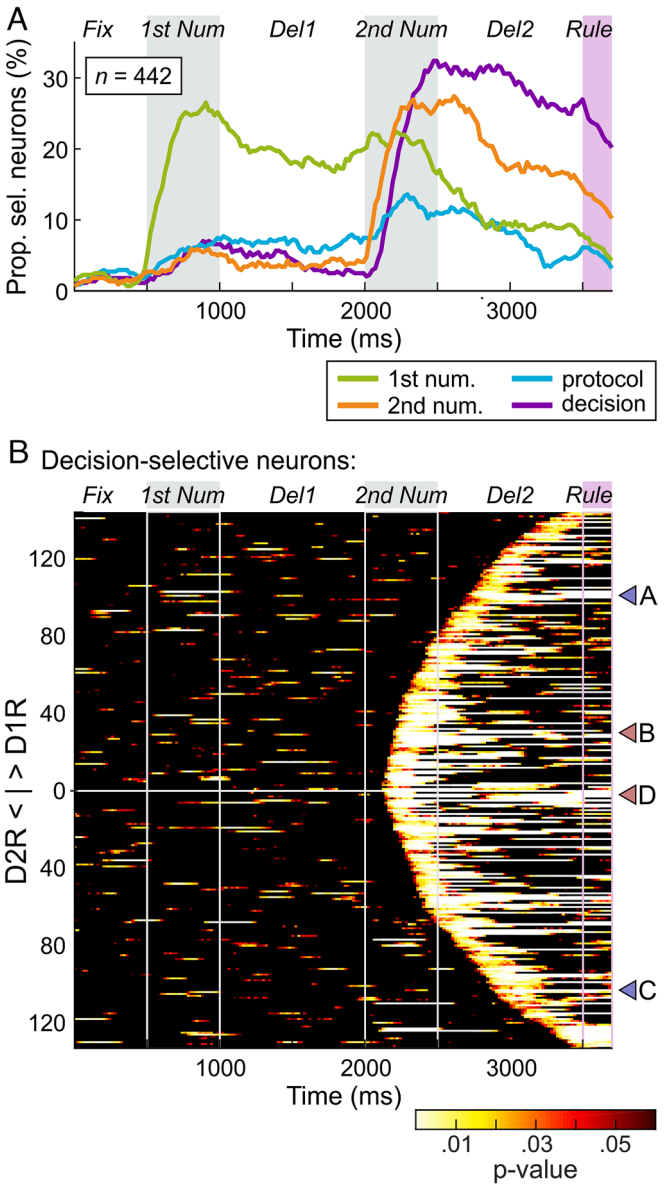

Fig. 4. Single neurons encode decision information dynamically. (*A*) Proportion of neurons that are selective for different task factors during the course of the trial. (*B*) Temporal profiles of all decision-selective neurons, sorted by latency of decision encoding, for units modulated by a D1R agonist (*Top*) or D2R agonist (*Bottom*). Each row shows the *P*-values of a unit for the factor "decision" in the sliding-window 4-factor LME, bright colors corresponding to significant intervals. The labeled triangles on the *Right* refer to the example units shown in Fig. 3.

We first identified time windows of significant above-chance classification (Fig. 6 *A* and *D*) by comparing decoding accuracies at each time step against a null distribution generated with shuffled labels ($\alpha = 0.01$). As expected, decoding accuracies hovered around chance (50%) during the early phases of the task. During the decision period (Delay 2), decoders showed strong and sustained performance (~75 to 85% in baseline conditions) for both D1R-modulated neurons (2,120 to 3,700 ms) and D2R-modulated neurons (2,200 to 3,700 ms).

Next, we compared the temporal dynamics of decoding accuracies between baseline and drug conditions within periods of significant decision coding. For the D1R-modulated population, a long interval of significant differences emerged at the end of the trial (3,220 to 3,680 ms; Fig. 6*A*). Consistent with the single-neuron results, decoding using average firing rates within the significant time window revealed significantly lower classifier performance under drug conditions (ΔAccuracy = –12.4% ± 1.3%; $P = 1.2733 \times 10^{-5}$, $Z = 4.3646$; two-sided Wilcoxon signed-rank test; $n = 30$ subsamples; *Methods*; Fig. 6 *B* and *C*). In contrast, D2R-modulated neurons showed the opposite pattern. A long interval of significant differences occurred at the start of the decision period (2,300 to 2,900 ms; Fig. 6*D*) during which decoding accuracy under drug conditions was significantly higher (ΔAccuracy = 7.6% ± 1.0%; $P = 3.4571 \times 10^{-5}$, $Z = -4.1411$; Fig. 6 *E* and *F*).

Dopamine Modulates Dynamics of Population Decision Codes. The transient maintenance and manipulation of task-relevant information is a hallmark of working memory. Emerging evidence suggests that working memory representations partly arise from dynamic populations exhibiting mixed selectivity, diverse onset latencies, and temporally transient tuning profiles (20, 21, 54–56). This dynamic code thus complements the classic static code, in which neurons exhibit sustained selectivity throughout the working-memory delay period (57, 58).

We hypothesized that dopamine modulates neuronal decision codes, shifting population activity from a dynamic to a more static format, or vice versa. To assess how dopamine receptor stimulation influenced population coding dynamics, we applied temporal generalization analysis (59) and performed a cross-temporal classifier decoding analysis. Classifiers were trained and tested on neuronal firing rates across time within the decision period (from the onset of the second numerosity to the end of Delay 2), yielding a cross-temporal decoding matrix comparing training and testing times (*Methods*). If information is encoded in a static format, classifiers generalize across time, yielding a square-like pattern of uniform decoding accuracy in the cross-temporal matrix. In contrast, a dynamic code produces high accuracy confined to temporally adjacent time points along the diagonal (59).

In baseline conditions without drug applications, decoding accuracy peaked along the diagonal of the matrix—where training and test times were identical—while most off-diagonal elements showed reduced but still above-chance performance (Fig. 7 *A* and *B*, *Upper*). This pattern indicates that population activity evolved dynamically over time.

To assess how drug application influenced coding dynamics, we performed temporal generalization analyses separately for baseline and drug trials, comparing D1R- (Fig. 7*A*) and D2R-stimulation (Fig. 7*B*) effects within their respective neuronal subpopulations. For each subpopulation and drug condition, we identified regions of generalizable coding, defined as contiguous time points that were significantly above chance.

We found that D1R-stimulation (SKF81297) significantly reduced the area of generalizable coding in the cross-temporal decoding matrix ($P = 3.12 \times 10^{-9}$, $t = -7.2116$; two-sided one-sample *t* test against zero). Consequently, high-accuracy values became confined to the diagonal, indicating a shift toward a more dynamic coding regime under D1R stimulation (Fig. 7 *C*, *Left*).

In contrast, D2R-stimulation (quinpirole) significantly increased the area of generalizable coding in the cross-temporal decoding matrix ($P = 1.23 \times 10^{-11}$, $t = 8.7873$). Thus, high-accuracy values extended beyond the diagonal, producing a more square-like pattern and indicating a shift toward a more static coding regime under D2R stimulation (Fig. 7 *C*, *Right*).

We quantified drug-induced changes in coding dynamics by comparing the extent of coding regions between baseline and drug trials. For each subpopulation, this was measured as the difference between time points on the matrix classified as generalizable in baseline but not in drug, and vice versa. Under D1R stimulation, values

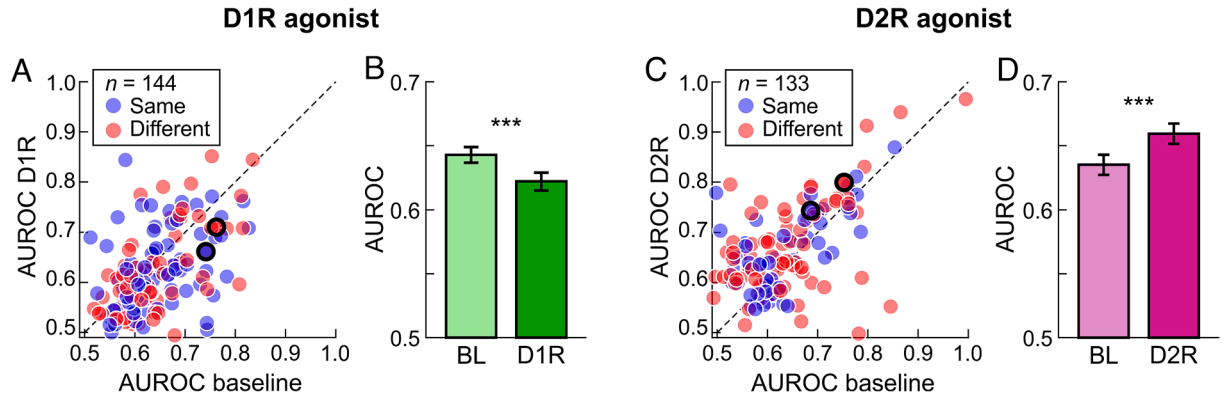

Fig. 5. Dopamine receptors exert opposite effects on neuronal decision selectivity. (*A*) Decision discriminability (AUROC) under baseline vs. D1R stimulation during intervals of significant decision encoding. Each point corresponds to one neuron; colors indicate the preferred decision. The black-bordered points refer to the example units shown in Fig. 3 *A* and *B*. (*B*) Average decision discriminability (AUROC) during BL trials and D1R stimulation (n = 144 neurons). ***P < 0.001 (two-sided Wilcoxon signed-rank test); bars depict mean ± SEM. (*C*) Decision discriminability (AUROC) compared between baseline and D2R stimulation during intervals of significant decision encoding. Same conventions as in *A*. The black-bordered points refer to the example units shown in Fig. 3 *C* and *D*. (*D*) Average decision discriminability (AUROC) during BL trials and D2R stimulation (n = 133 neurons). Same conventions as in *B*.

characterizing the change in temporal coding dynamics, the change in generalizable areas (ΔGA), shifted significantly toward negative, confirming a transition to a more dynamic code (ΔGA = −29.92, $P = 2.58 \times 10^{-4}$; Fig. 7*D*). In contrast, D2R stimulation shifted values significantly toward positive, reflecting a shift toward static coding (ΔGA = 91.78, $P = 2.85 \times 10^{-18}$; Fig. 7*D*). The changes in temporal coding dynamics were also different between D1R stimulation and D2R stimulation ($P = 6.47 \times 10^{-21}$; Fig. 7*D*).

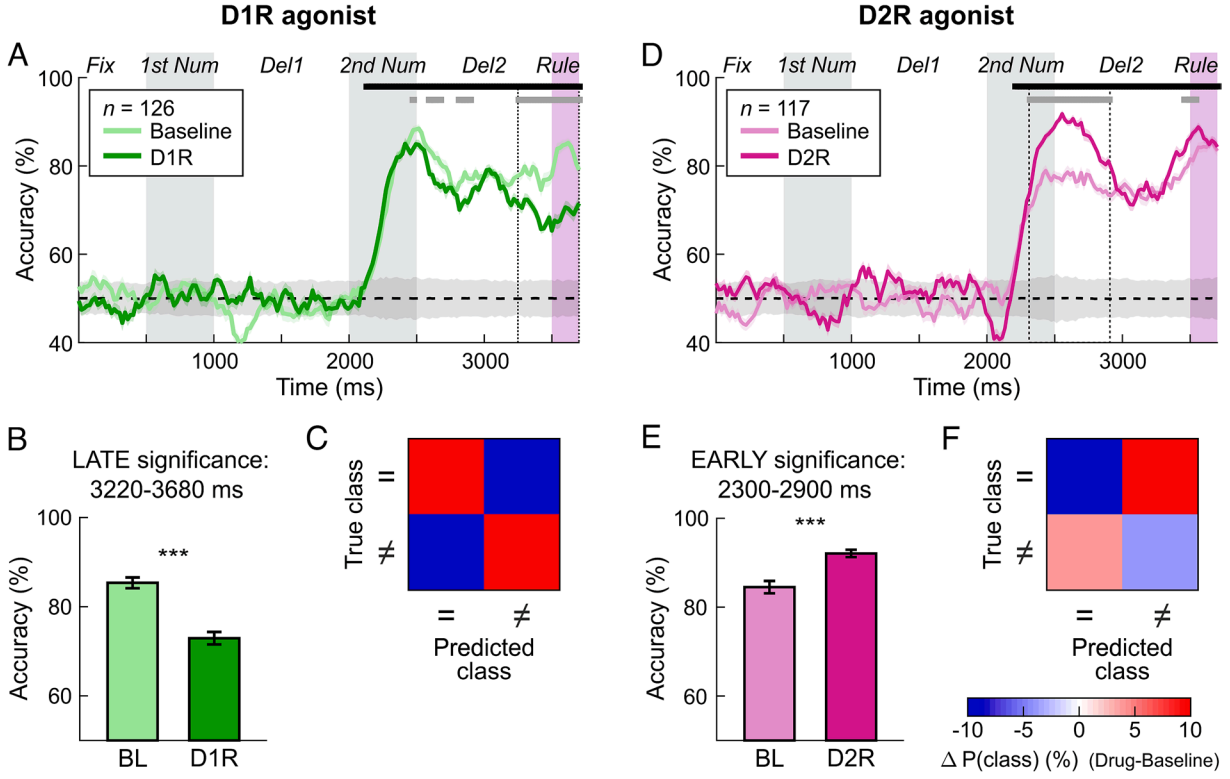

Fig. 6. Dopamine receptor stimulation bidirectionally modulates population decision decoding. (*A*) Classification accuracy for decoding decision information during baseline and drug trials, respectively, after training SVM classifiers on instantaneous firing rates of D1R-modulated neurons (n = 126) across the entire trial period. The black dashed line shows average accuracy of classifiers trained on shuffled data (matching the chance level of 50% for two classes); the gray shaded area depicts the 99th percentile of that distribution ($n_{permutations}$ = 1,000). The thickened black bar above the data indicates the interval when the true accuracies of both drug conditions differ significantly from accuracies obtained for shuffled labels (P < 0.01; permutation test). The thickened gray bars indicate time steps at which accuracies differ significantly between baseline and drug condition (P < 0.01; two-sided Wilcoxon signed-rank test). (*B*) Average accuracies for BL trials and trials of D1R stimulation, when training SVM classifiers on firing rates averaged across the longest interval of significant differences between drug conditions (thickened gray bar and dashed black square in *A*). ***P < 0.001 (two-sided Wilcoxon signed-rank test); bars depict mean ± SEM across subsamples (n = 30). (*C*) Difference in decoder performance (probability of predicting the correct decision condition) between baseline and drug trials in the fixed-window analysis described in *B*. (*D*) Classification accuracy for decoding decision information during baseline and drug trials, respectively, after training SVM classifiers on instantaneous firing rates of D2R-modulated neurons (n = 117). Same conventions as in *A*. (*E*) Average accuracies for BL trials and trials of D2R stimulation, when training SVM classifiers on firing rates averaged across the longest interval of significant differences between drug conditions (thickened gray bar and dashed black square in *D*). Same conventions as in *B*. (*F*) Difference in decoder performance (probability of predicting the correct decision condition) between baseline and drug trials in the fixed-window analysis described in *E*.

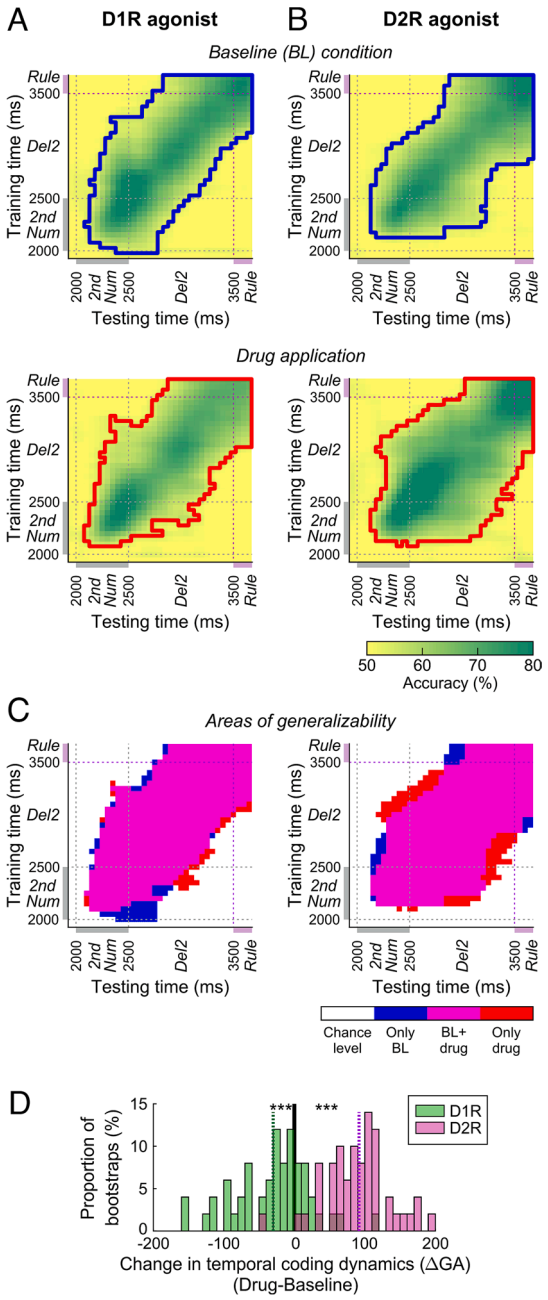

Fig. 7. Dopamine receptor stimulation opposingly modulates the cross-temporal decision coding dynamics. (*A*) Cross-temporal classification accuracy for decoding decision information in baseline trials (*Upper*) and during drug application (*Lower*), respectively, for subpopulations of D1R-modulated neurons when training SVM classifiers on instantaneous firing rates at a given time point and testing on another one (the main diagonals of the matrices correspond to the curves in Fig. 6*A*). Thick contours indicate significant differences from chance level ($P < 0.01$; permutation test) in baseline and drug conditions, respectively. (*B*) Cross-temporal classification accuracy for subpopulations of D2R-modulated neurons during baseline (*Upper*) and drug (*Lower*) conditions, respectively (the main diagonals of the matrices correspond to the curves in Fig. 6*D*). Same conventions as in *A*. (*C*) Areas of significant cross-temporal coding for D1R-modulated neurons (*Left*) and D2R-modulated neurons (*Right*). Pink areas indicate coding in both baseline and drug condition; blue and red areas indicate significance only during baseline trials or drug application, respectively. Figure legend: "Only BL," generalizability only in baseline trials; "BL + drug," generalizability in both baseline and drug trials; "Only drug," generalizability only in the respective drug trials. (*D*) Changes in coding for neurons modulated by a D1R agonist (green) or a D2R agonist (pink), quantified by subtracting the number of blue matrix elements in *C* (i.e., time points of coding only during baseline trials) from the number of red matrix elements in *C* (i.e., time points of coding only during drug application). ***$P < 0.001$ (two-sided one-sample *t* test against zero); the dashed vertical lines depict the median across bootstraps ($n = 50$).

These findings suggest that PFC neurons become more transiently selective during the decision-delay period under D1R stimulation, and more persistently selective under D2R stimulation. To confirm this conclusion, we modeled a population of artificial neurons, each tuned to one of two memoranda (same/different). To simulate the observed drug effects, we systematically varied the duration of significant stimulus discrimination, i.e., the artificial neurons' sustained tuning duration (*SI Appendix*, Fig. S2*A* and *Methods*), and reran the full cross-temporal support vector machine (SVM) analysis using artificial neurons with different selectivity intervals.

When the neurons' tuning duration was very short, the coding area in the temporal generalization matrix remained contracted around the diagonal as expected for a dynamic code based on transiently tuned neurons (*SI Appendix*, Fig. S2 *B*, *Left*). This replicated the effects of D1R stimulation observed in PFC decision-related neurons (Fig. 7 *C* and *D*).

Conversely, when the neurons' tuning duration grew longer and became more sustained, the partially generalizable coding area became increasingly expanded (*SI Appendix*, Fig. S2 *B*, *Right*). This replicated the effects of D2R stimulation observed in PFC neurons. The correspondence of the model and observed results suggest that D1R stimulation shifts the population code toward a more dynamic regime by making neuronal selectivity more temporally transient, whereas D2R stimulation promotes a more static code by extending neuronal selectivity over time.

Discussion

In this study, we investigated how dopamine D1 and D2 receptor signaling in the primate dorsolateral prefrontal cortex (dlPFC) modulates the encoding of abstract, response-independent numerical decisions. By combining single-neuron recordings with microiontophoretic drug application during a delayed numerical comparison task, we provide direct electrophysiological evidence that D1R and D2R activation exert complementary yet opposing influences on both the strength and temporal dynamics of prefrontal cognitive representations.

Although we did not directly test saline-only positive ejection currents in the current study, our previous experiments using the same iontophoretic apparatus and protocols indicate that the observed neuronal effects were not caused by current injection. Across four prior studies in monkey PFC, saline-only injections of 0.9% NaCl with ejection currents between +25 nA and +50 nA had no impact on neuronal firing rates or coding during sensory or delay phases (43, 44, 52, 60). Collectively, these results confirm that the dopaminergic effects reported here cannot be attributed to nonspecific electrical currents. Our key findings, discussed in detail below, reveal a bidirectional and receptor-specific control of abstract decision coding in the dlPFC.

First, we found that D1 receptor (D1R) stimulation late in the trial suppressed, whereas D2 receptor (D2R) stimulation early in the trial enhanced the decision-coding strength of single prefrontal neurons during the maintenance of abstract decisions. These opposing effects extended to the population level, where D1R and D2R activation exerted complementary influences on both the decodability and temporal structure of neural representations. Specifically, D1R stimulation reduced population-level decoding accuracy, while D2R stimulation enhanced it, indicating a bidirectional modulation of representational strength and stability. This result aligns with prior evidence that D1Rs can sharpen selectivity in a dose-dependent manner, effectively filtering irrelevant inputs and stabilizing network representations (23, 37–39). Conversely,

D2R activation has been shown to increase neuronal excitability and support flexible updating of working memory content, consistent with the enhancement of decision discriminability observed here (42–44). Importantly, these opposing effects support a receptor-specific mechanism for balancing cognitive stability and flexibility: D1Rs may constrain neuronal activity to reduce interference late in the decision period, while D2Rs broaden the dynamic range of network responses to facilitate adaptation to changing task demands early in the decision period (29, 45).

Our results extend these previous findings by demonstrating that such modulation is not limited to spatial or feature-based working memory, but also applies to abstract, action-independent decision signals, providing direct evidence that dopamine receptor subtypes selectively shape the encoding of cognitively computed judgments in PFC populations.

Second, and perhaps even more importantly, our results show that dopamine receptor activation bidirectionally modulates the temporal structure of the decision code within the working-memory buffer. D1R stimulation shifted neural activity toward a more dynamic and transient regime, characterized by temporally confined firing and mixed selectivity across neurons (19–22). In contrast, D2R stimulation promoted a more stable and persistent coding regime, extending the duration of decision-selective activity throughout the delay period and reinforcing the maintenance of abstract representations over time (13, 15–18). These findings provide direct neurophysiological evidence that receptor-specific dopamine signaling shapes the temporal architecture of working-memory-based decision representations (59).

These findings extend and refine the dual-state theory of prefrontal dopamine function (25, 29, 36) by demonstrating that receptor-specific dopamine signaling not only modulates single-neuron selectivity but also reorganizes the temporal dynamics of population activity within prefrontal ensembles. Consistent with this framework, D1Rs and D2Rs exert opposing influences at the population level: D1R activation weakens decision coding and promotes more transient coding which could give rise to temporal flexibility, enabling the network to dynamically filter distractions while flexibly updating decision-relevant information. D2R, on the other hand, enhances temporal stability, seemingly fostering sustained, attractor-like activity that preserves information across delays (39, 44). Interestingly, the direction of this pattern diverges from the classical predictions of the dual-state theory for working memory, which posit that D1R activation stabilizes and D2R activation destabilizes network states (25, 29, 36).

We hypothesize that the divergence from classical dual-state predictions reflects a circuit- and task-specific interaction between D1R and D2R modulation. In abstract decision circuits, D1R activation may selectively enhance transient tuning producing more confined, dynamic patterns, whereas D2R activation may promote more persistent tuning producing more static patterns (21, 37, 45). These effects suggest that the mapping from receptor type to coding dynamics is context-dependent and may differ from the canonical PFC working-memory regime on which the dual-state theory is based. This proposes that the dual-state theory should be expanded to incorporate such context-dependent effects, recognizing that dopamine regulates not only attractor stability but also the temporal structure and persistence of population activity (37, 44, 45).

These findings provide insight into how D1R- and D2R-mediated signaling shapes population coding in prefrontal circuits, with potential relevance for theories of schizophrenia (45, 61–65). However, because our results are based on acute, local pharmacological manipulations in dlPFC during a specific decision-making task, they do not directly model the chronic and distributed dopaminergic dysfunction associated with schizophrenia. In our data, increased D2R activation enhanced population coding strength and promoted more persistent, temporally stable representations, whereas reduced D2R activation weakened stability and reliable readout. In contrast, D1R activation reduced decision-coding strength at the single-neuron level and shifted population activity toward more transient, temporally restricted coding, whereas reduced D1R activity weakened decision coding and diminished temporal flexibility (37, 39, 66). Together, these observations highlight receptor-specific influences on the dynamic–static balance of prefrontal population codes and provide a hypothesis-generating framework for how disruptions in D1R or D2R signaling could impact cognitive and perceptual processes.

In conclusion, our study demonstrates that dopamine in the dlPFC acts as a versatile modulator of high-level cognitive representations, tuning not only the strength but also the temporal format of abstract decision codes. The complementary actions of D1 and D2 receptors provide a mechanistic basis for the fine balance between cognitive stability and flexibility. Future work should explore how these receptor-specific modulation patterns interact with other neuromodulators and how they are engaged by different cognitive demands to enable the rich repertoire of executive functions supported by the PFC.

Methods

Animals. Two adult male rhesus monkeys (*Macaca mulatta*, monkey M1, 10 y old, and monkey M2, 7 y old) served as subjects for this experiment. Subject details and experimental procedures have been reported previously (11), and were in accordance with the guidelines for animal experimentation approved by the national authority, the Regierungspräsidium Tübingen, Germany.

Surgery. Both monkeys were implanted with titanium head posts and recording chambers over the principal sulcus, anterior to the frontal eye fields: M1 had chambers on the left and right hemispheres, and M2 on the left hemisphere. Implantation surgeries were conducted under general anesthesia using aseptic techniques (11). Before surgery, anatomical MRI was performed to locate anatomical landmarks and to reconstruct recording sites via stereotaxic coordinates.

Experimental Setup. During experiments, the monkeys were head-restrained, seated in primate chairs, and positioned 57 cm in front of a flat-screen monitor (15 in, 1,024 × 768 display resolution at 75 Hz) within darkened experimental chambers. To present stimuli and collect behavioral data we used the CORTEX program (NIMH, Bethesda, MD); eye-tracking data were monitored continuously and sampled within trials using an infrared tracking system (ISCAN, Woburn, MA). Responses were registered using a custom-fitted touch-responsive bar in the primate chair, and sampled by CORTEX through a touch monitoring system (Crist Instruments, Hagerstown, MD). Upon successful completion of each trial, monkeys received fluid rewards from a gravity dispenser controlled by a solenoid valve system (Crist Instruments, Hagerstown, MD) connected to CORTEX.

Experimental Task and Stimuli. Monkeys were trained on a numerical same-different decision task (Fig. 1*A*). To initiate a trial, the subjects had to grab the response bar and fixate the fixation spot in the center of a gray circle. They had to maintain fixation throughout the trial and hold the response bar until a response was appropriate.

After a 500 ms fixation period, the first dot display was shown for 500 ms, followed by a delay period of 1,000 ms during which the stimulus was removed. The numerosity of this stimulus had to be remembered and compared against the numerosity of a second dot display which was presented subsequently for 500 ms and followed by another delay period of 1,000 ms. Only then the monkeys could decide whether the two stimulus displays contained the same or different numbers of dots. Afterward, a colored square would follow (presented for <800 ms) that instructed the monkeys how to respond: The red rule indicated bar release if different, and hold if same; the blue rule indicated the opposite, i.e., bar release if same, and hold if different. If the monkeys paired decision (same/different)

and rule (red/blue) with the correct motor response (release/hold), they received a liquid reward. Erroneous trials ended in a time-out of 1 to 2 s.

Numerosity stimuli depicted black dots on a gray background circle, and were newly generated before every session using custom-written MATLAB scripts. Both first and second number stimuli contained 1, 3, or 9 dots in two different stimulus protocols to control for low-level visual features. That is, the "standard" protocol consisted of black dots with randomly chosen radii and spacing; the "control" protocol ensured the same total black area (by controlling the dot radii) and density of all items. Rule cues showed a red or blue square, respectively, in the center of the gray circle.

Five factors were varied systematically: First numerosity (1,3,9), decision (same/different), second numerosity (1,3,9; chosen so that "same" and "different" trials were counterbalanced, e.g., 1–1, 1–1, 1–3, 1–9), stimulus protocol (standard/control), and rule cue (red/blue); resulting in 48 unique conditions. Blocks of 48 unique trials in which all factors were pseudorandomized were presented alternatingly for baseline and drug conditions. In total, 114 sessions (M1: 57 sessions, M2: 57 sessions) were recorded.

Electrophysiological Recording and Iontophoretic Drug Application. Extracellular recordings and microiontophoretic drug application were performed as described previously (37, 38, 43, 52, 60). In each recording session, up to three custom-made tungsten-in-glass electrodes (67) with two flanking pipettes each were lowered transdurally into the brain using a modified electrical microdrive (NAN Instruments, Nazaret Illit, Israel). We randomly recorded single neurons and made no attempts to preselect the cells according to any task-related activity or based on drug effects. Signal acquisition, filtering, amplification, and digitization were accomplished with the MAP system (Plexon, Dallas, TX); waveform separation was performed offline (Offline Sorter, Plexon, Dallas, TX).

Drugs were applied iontophoretically (MVCS iontophoresis system, npi electronic, Tamm, Germany) using the aforementioned custom-made tungsten-in-glass electrodes. Electrode impedance and pipette resistance were measured after each recording session. Electrode impedances were 0.8 to 3.0 MΩ (measured at 500 Hz; Omega Tip Z; World Precision Instruments, Sarasota, FL). Typical pipette resistances were 15 to 50 MΩ (full range, 12 to 160 MΩ), and depended on the pipette opening diameter, drug, and solvent used. Only one drug was tested per recording session, that is, either the D1 receptor (D1R) agonist SKF81297 (Sigma-Aldrich, Munich, Germany) or the D2 receptor (D2R) agonist quinpirole (Sigma-Aldrich, Munich, Germany). These drugs are highly selective and show very little affinities for the corresponding other receptor family (68). At the same time, they are highly specific and show little affinity to other receptors such as serotonin receptors (69, 70). Both drugs were dissolved in ultrapure, double distilled water at a concentration of 10 mM and a pH of 4.0 using HCl, respectively, and filled into one barrel of the electrodes. The other barrel was always filled with 0.9% physiological NaCl to prevent excess drug solution to spill over into this barrel during the filling process. As in previous experiments (37, 43, 44, 52, 60), retention currents of −7 nA were used to hold the drugs in the pipette during baseline conditions. The ejection current for SKF81297 was +15 nA, the one for quinpirole was +40 nA. The different effective ejection currents for SKF81297 and quinpirole are likely related, at least in part, to differences in receptor affinity and pharmacological properties of D1- vs. D2-like receptor agonists, although additional factors such as tissue diffusion, receptor density, and signaling efficacy may also contribute. We did not investigate dosage effects and chose ejection currents to match the values reported to be maximally effective, that is, in the peak range of the "inverted-U function" (39, 71).

In each recording session, blocks of baseline conditions (using the retention currents) alternated with blocks of drug application (using the ejection currents) until the monkeys were saturated and stopped working. Drugs were applied continuously for 12 to 15 min, depending on the number of trials completed correctly by the animal. The first block was always the baseline condition. Given that iontophoretic drug application is fast and can quickly modulate neuronal firing properties (52), we did not exclude data at the current switching points.

Data Analysis. All data analysis was performed using custom-written scripts in the MATLAB computational environment (Mathworks). A total of 442 well-isolated single neurons (M1: 166 neurons; M2: 276 neurons) entered the analysis: We recorded 235 cells during D1R stimulation and 207 cells during D2R stimulation. Each of these neurons was recorded for at least 30 trials for baseline and drug condition, respectively, and fired with an average spike rate above 0.5 Hz over the entire trial period of 3,700 ms (from fixation onset to 200 ms after the onset of the rule cue stimulus). Only correct trials were included in the analyses. Neurons were not preselected based on drug effects.

Decision neurons. To test neuronal discrimination behavior, we performed an LME regression analysis for each cell using a model of the form *FRs ~ 1st num. + 2nd num. + protocol + decision* (Wilkinson notation). To assess the temporal evolution of signals, spike trains were smoothed trial-wise (Gaussian kernel with $\sigma = 150$ ms; total window size: 300 ms) within the entire trial period. Using a step size of 20 ms, instantaneous firing rates were then subjected to the LME model, resulting in a temporal sequence of *P*-values for each of the four factors.

We identified intervals of significant encoding by determining temporal "clusters" during which the *P*-values of a certain factor were above threshold ($\alpha = 0.05$) for at least 10 consecutive steps. A neuron was then termed "decision neuron" if a significant cluster for the factor "decision" was observed during the task-relevant time window, i.e., 2,100 to 3,400 ms (onset of 2nd number stimulus to 200 ms before Delay 2 offset, shifted by 100 ms response latency); if, additionally, there were no concurrent or overlapping significant intervals for any of the remaining three factors, the neuron was termed "pure decision neuron."

Receiver operating characteristics (ROC) analysis. To quantify each neuron's coding strength, we performed an ROC analysis (72), derived from signal detection theory. The area under the ROC curve (AUROC) denotes the probability with which an ideal observer can tell apart a meaningful signal from a noisy background, thus providing a nonparametric measure for the discriminability of two distributions. Values of 0.5 indicate no separation, and values of 1.0 signal perfect discriminability. As the ROC takes into account both the difference between distribution means as well as their widths, it is a suitable indicator of signal quality (73).

For each neuron, we calculated the spike rates for "same" and "different" trials, respectively, by averaging activity within the interval of significant decision coding. In case we observed multiple significant clusters (60/277 neurons), discharge rates were calculated based on the longest interval. The condition that elicited higher responses was determined as the "preferred" decision. Discriminability was then quantified by calculating the AUROC based on the firing rate distributions for preferred and nonpreferred decision.

To evaluate the impact of drug application, baseline and drug conditions were analyzed separately for each drug, and then compared using two-sided Wilcoxon signed-rank tests.

Decoding analysis. For the decoding analysis, we trained SVMs, as implemented by the MATLAB function *fitcecoc*, to distinguish between the two classes "same" and "different" decision. Neurons stimulated by the same drug were treated as a pseudopopulation; within each of these populations, baseline and drug trials were analyzed separately.

To ensure comparable training and the same impact for all task features, trials were rigorously balanced for the factors "1st num.," "2nd num.," "protocol," and "decision." Note, that for each sample numerosity, there are two "different" sample–test stimulus pairs (e.g., 1–3 and 1–9), but only one "same" sample–test stimulus pair (e.g., 1–1). To account for this inevitable imbalance, each of the 12 "different" conditions had to occur at least two times, and each of the six "same" conditions had to occur at least four times, resulting in 24 trials per class. Cells for which we did not record enough trials per condition were excluded from the analysis. This check gave us a final pseudopopulation of 126 (out of 235) D1R-modulated neurons, and 117 (out of 207) D2R-modulated cells.

To assess the temporal evolution of signals, instantaneous firing rates were sampled at a step size of 20 ms, smoothing spike trains trial-wise using a Gaussian kernel with $\sigma = 150$ ms (total window size: 300 ms). All firing rates were then normalized by z-scoring (obtaining mean and SD from training data only). For each drug (D1R/D2R agonist) and drug condition (baseline/drug), we ran 30 runs of decoding, each time using a different subset of randomly sampled trials per condition. Within each run, we applied fourfold cross-validation, i.e., 36 trials were used as training set and the remaining 12 trials were used as test set, balancing conditions within each set. Decoder performance was then quantified as the percent of held-out test trials correctly classified as "same" or "different" (accuracy), averaged across the 30 runs.

We repeated the entire decoding analysis with 1,000 permutations using shuffled trial labels, to get a null distribution of classifier performance. Intervals of significant decision decoding were then defined as those temporal "clusters" during which the sequences of true accuracies were above the 99th percentile

of the null distribution for at least 10 consecutive steps, for both baseline and drug condition.

To evaluate the impact of drug application within the time window of significant decision decoding (D1R: 2,120 to 3,700 ms; D2R: 2,200 to 3,700 ms), we compared the accuracies between baseline and drug conditions across the 30 runs at every time step using two-sided Wilcoxon signed-rank tests ($\alpha = 0.01$). For both D1R- and D2R-agonist, we observed a time window during which accuracies were significantly modulated by the drug for more than 10 consecutive steps (D1R: 3,220 to 3,680 ms; D2R: 2,300 to 2,900 ms). To quantify these modulation differences more specifically, we performed additional fixed-window SVM analyses (using the same selection criteria and parameters as above) based on the average firing rates within the significant time windows, for baseline and drug conditions, respectively. We then assembled a confusion matrix, which counts the frequency at which a trial of a certain class is assigned different labels by the classifier.

Cross-temporal coding dynamics. To investigate the cross-temporal evolution of information coding, we repeated the decoding analysis described before, this time, however, training and testing the SVM classifiers on all possible combinations of time points (sampled at a step size of 50 ms). This results in a two-dimensional cross-temporal decoding matrix (*CTD*) of accuracies spanning time points of classifier training against time points of classifier testing, i.e., the values along the diagonal correspond to time points identical for training and testing. As before, the entire procedure was repeated 30×, each time randomly resampling trials; then, the results were averaged over the cross-validations and these 30 runs.

To identify areas of coding generalizability, i.e., with significant above-chance accuracy (50% for two classes), we performed a cluster permutation test (74). In short, we repeated the entire analysis with 1,000 permutations of randomly shuffled trial labels ($\alpha_{clus} = 0.01$). Then, we compared the true accuracy values against this null distribution of classifier performance at every time point, and identified "clusters" of connected significant matrix elements in the *CTD*. These "cluster candidates" were then evaluated by comparison with clusters observed for the shuffled data ($p_{rank} < 1\%$).

The cluster permutation test results in a binary matrix (generalizable areas, *GA*) of the same dimensions as *CTD*, denoting for every time point whether it is classified as generalizable (1) or not (0). The size of the generalizable areas, i.e., the sum of all significant elements in the GA matrix, provides a relative measure for the temporal dynamics of the population code.

To quantify how drug application may alter the temporal coding dynamics, we computed the *GA* matrix separately for baseline and drug conditions, for the neuronal subpopulations of D1R- and D2R-modulated cells, respectively. Within each subpopulation, we then determined the relative complement of GA_{Ctrl} and GA_{Drug}, respectively (i.e., we counted all time points classified as generalizable during baseline conditions, but not during drug application, and vice versa), and took the difference between these two values as a measure for the change in temporal coding dynamics ΔGA of that particular subpopulation.

$$\Delta GA = \Sigma\left(\frac{GA_{Drug}}{GA_{Ctrl}}\right) - \Sigma\left(\frac{GA_{Ctrl}}{GA_{Drug}}\right).$$

As the classifier's performance can be influenced by the size of the population used, and to estimate a distribution of the change in coding dynamics, we applied a bootstrapping test. That is, we repeated the entire cross-temporal decoding analysis 50×, each time randomly subsampling 100 neurons from the population of D1R- and D2R-modulated cells, respectively. That way we obtained 50 ΔGA values for each subpopulation, which were then compared using two-sided one-sample *t* tests.

Neuronal Population Model. To investigate how variable onset latencies and tuning durations alter the appearance of the temporal generalization matrix, we modeled a population of artificial neurons, tuned to either "same" or "different," and reran the entire cross-temporal SVM analysis. The density curves of the individual neurons were modeled so that baseline firing rates, amplitude, and activity difference between the two conditions were comparable to those of the biological data; onset latencies were evenly spaced across the "decoding window," the tuning durations were varied systematically from 100 to 500 ms (*SI Appendix*, Fig. S1*A*). That way we generated a pool of 160 units, each with 40 trials. For the cross-temporal SVM analysis, we randomly sampled 100 units with 24 trials each, and used the same classifier parameters as described above. The cross-temporal generalization matrix and areas of generalizable coding were then determined as before. Data and software data are available for download from GitHub (75).

Data, Materials, and Software Availability. Data and software data have been deposited in github (https://github.com/EstherKutter/Dopamine-D1-and-D2-Receptors-Differentially-Control-Abstract-Decision-Codes-in-Primate-PFC) (75). All other data are included in the manuscript and/or *SI Appendix*.

ACKNOWLEDGMENTS. This work was supported by a DFG Grant NI 618/13-1 (FOR 5159) to A.N.

Author affiliations: [a]Animal Physiology, Institute of Neurobiology, Department of Biology, University of Tuebingen, Tuebingen 72076, Germany

1. J. Fuster, *The Prefrontal Cortex* (Academic Press, ed. 4, 2008).
2. E. K. Miller, J. D. Cohen, An integrative theory of prefrontal cortex function. *Annu. Rev. Neurosci.* **24**, 167–202 (2001).
3. A. K. Churchland, R. Kiani, Three challenges for connecting model to mechanism in decision-making. *Curr. Opin. Behav. Sci.* **11**, 74–80 (2016).
4. J. N. Kim, M. N. Shadlen, Neural correlates of a decision in the dorsolateral prefrontal cortex of the macaque. *Nat. Neurosci.* **2**, 176–185 (1999).
5. M. N. Shadlen, R. Kiani, Decision making as a window on cognition. *Neuron* **80**, 791–806 (2013).
6. S. Bongard, A. Nieder, Basic mathematical rules are encoded by primate prefrontal cortex neurons. *Proc. Natl. Acad. Sci. U.S.A.* **107**, 2277–2282 (2010).
7. S. L. Brincat, M. Siegel, C. von Nicolai, E. K. Miller, Gradual progression from sensory to task-related processing in cerebral cortex. *Proc. Natl. Acad. Sci. U.S.A.* **115**, E7202–E7211 (2018).
8. D. J. Freedman, J. A. Assad, Neuronal mechanisms of visual categorization: An abstract view on decision making. *Annu. Rev. Neurosci.* **39**, 129–147 (2016).
9. D. Mendoza-Halliday, S. Torres, R. Desimone, J. Martinez-Trujillo, Functional and anatomical characterization of visual working memory coding. *J. Vis.* **18**, 106–106 (2018).
10. K. Merten, A. Nieder, Active encoding of decisions about stimulus absence in primate prefrontal cortex neurons. *Proc. Natl. Acad. Sci. U.S.A.* **109**, 6289–6294 (2012).
11. P. Viswanathan, A. M. Stein, A. Nieder, Sequential neuronal processing of number values, abstract decision, and action in the primate prefrontal cortex. *PLoS Biol.* **22**, e3002520 (2024).
12. J. D. Wallis, K. C. Anderson, E. K. Miller, Single neurons in prefrontal cortex encode abstract rules. *Nature* **411**, 953–956 (2001).
13. J. M. Fuster, G. E. Alexander, Neuron activity related to short-term memory. *Science* **173**, 652–654 (1971).
14. K. Kubota, H. Niki, Prefrontal cortical unit activity and delayed alternation performance in monkeys. *J. Neurophysiol.* **34**, 337–347 (1971).
15. F. Ceccarelli *et al.*, Static and dynamic coding in distinct cell types during associative learning in the prefrontal cortex. *Nat. Commun.* **14**, 8325 (2023).
16. S. Funahashi, C. J. Bruce, P. S. Goldman-Rakic, Mnemonic coding of visual space in the monkey's dorsolateral prefrontal cortex. *J. Neurophysiol.* **61**, 331–349 (1989).
17. P. S. Goldman-Rakic, Cellular basis of working memory. *Neuron* **14**, 477–485 (1995).
18. L. Thrower, W. Dang, R. G. Jaffe, J. D. Sun, C. Constantinidis, Decoding working memory information from neurons with and without persistent activity in the primate prefrontal cortex. *J. Neurophysiol.* **130**, 1392–1402 (2023).
19. M. Rigotti *et al.*, The importance of mixed selectivity in complex cognitive tasks. *Nature* **497**, 585–590 (2013).
20. E. Spaak, K. Watanabe, S. Funahashi, M. G. Stokes, Stable and dynamic coding for working memory in primate prefrontal cortex. *J. Neurosci.* **37**, 6503–6516 (2017).
21. M. G. Stokes *et al.*, Dynamic coding for cognitive control in prefrontal cortex. *Neuron* **78**, 364–375 (2013).
22. K. M. Tye *et al.*, Mixed selectivity: Cellular computations for complexity. *Neuron* **112**, 2289–2303 (2024).
23. A. F. T. Arnsten, Catecholamine influences on dorsolateral prefrontal cortical networks. *Biol. Psychiatry* **69**, e89–e99 (2011).
24. V. de Lafuente, R. Romo, Dopamine neurons code subjective sensory experience and uncertainty of perceptual decisions. *Proc. Natl. Acad. Sci. U.S.A.* **108**, 19767–19771 (2011).
25. D. Durstewitz, J. K. Seamans, The dual-state theory of prefrontal cortex dopamine function with relevance to catechol-o-methyltransferase genotypes and schizophrenia. *Biol. Psychiatry* **64**, 739–749 (2008).
26. T. Ott, A. Nieder, Dopamine and cognitive control in prefrontal cortex. *Trends Cogn. Sci.* **23**, 213–234 (2019).
27. M. V. Puig, E. K. Miller, The role of prefrontal dopamine D1 receptors in the neural mechanisms of associative learning. *Neuron* **74**, 874–886 (2012).
28. M. V. Puig, E. K. Miller, Neural substrates of dopamine D2 receptor modulated executive functions in the monkey prefrontal cortex. *Cereb. Cortex* **25**, 2980–2987 (2015).
29. J. K. Seamans, C. R. Yang, The principal features and mechanisms of dopamine modulation in the prefrontal cortex. *Prog. Neurobiol.* **74**, 1–58 (2004).
30. M. S. Lidow, P. S. Goldman-Rakic, D. W. Gallager, P. Rakic, Distribution of dopaminergic receptors in the primate cerebral cortex: Quantitative autoradiographic analysis using [3H]raclopride, [3H] spiperone and [3H]SCH23390. *Neuroscience* **40**, 657–671 (1991).

31. M. S. Lidow, F. Wang, Y. Cao, P. S. Goldman-Rakic, Layer V neurons bear the majority of mRNAs encoding the five distinct dopamine receptor subtypes in the primate prefrontal cortex. *Synapse* **28**, 10–20 (1998).
32. N. Santana, F. Artigas, Laminar and cellular distribution of monoamine receptors in rat medial prefrontal cortex. *Front. Neuroanat.* **11**, 87 (2017).
33. J. de Almeida, G. Mengod, D2 and D4 dopamine receptor mRNA distribution in pyramidal neurons and GABAergic subpopulations in monkey prefrontal cortex: Implications for schizophrenia treatment. *Neuroscience* **170**, 1133–1139 (2010).
34. E. C. Muly, K. Szigeti, P. S. Goldman-Rakic, D1 receptor in interneurons of macaque prefrontal cortex: Distribution and subcellular localization. *J. Neurosci.* **18**, 10553–10565 (1998).
35. J. F. Smiley, A. I. Levey, B. J. Ciliax, P. S. Goldman-Rakic, D1 dopamine receptor immunoreactivity in human and monkey cerebral cortex: Predominant and extrasynaptic localization in dendritic spines. *Proc. Natl. Acad. Sci. U.S.A.* **91**, 5720–5724 (1994).
36. D. Durstewitz, J. K. Seamans, T. J. Sejnowski, Neurocomputational models of working memory. *Nat. Neurosci.* **3**, 1184–1191 (2000).
37. S. N. Jacob, M. Stalter, A. Nieder, Cell-type-specific modulation of targets and distractors by dopamine D1 receptors in primate prefrontal cortex. *Nat. Commun.* **7**, 13218 (2016).
38. M. Stalter, S. Westendorff, A. Nieder, Dopamine gates visual signals in monkey prefrontal cortex neurons. *Cell Rep.* **30**, 164–172.e4 (2020).
39. S. Vijayraghavan, M. Wang, S. G. Birnbaum, G. V. Williams, A. F. T. Arnsten, Inverted-U dopamine D1 receptor actions on prefrontal neurons engaged in working memory. *Nat. Neurosci.* **10**, 376–384 (2007).
40. M. Wang *et al.*, NMDA receptors subserve persistent neuronal firing during working memory in dorsolateral prefrontal cortex. *Neuron* **77**, 736–749 (2013).
41. S. B. Floresco, O. Magyar, Mesocortical dopamine modulation of executive functions: Beyond working memory. *Psychopharmacol. (Berl.)* **188**, 567–585 (2006).
42. M. Klanker, M. Feenstra, D. Denys, Dopaminergic control of cognitive flexibility in humans and animals. *Front. Neurosci.* **7**, 201 (2013).
43. T. Ott, S. N. Jacob, A. Nieder, Dopamine receptors differentially enhance rule coding in primate prefrontal cortex neurons. *Neuron* **84**, 1317–1328 (2014).
44. T. Ott, A. Nieder, Dopamine D2 receptors enhance population dynamics in primate prefrontal working memory circuits. *Cereb. Cortex* **27**, 4423–4435 (2017).
45. R. Cools, The cost of dopamine for dynamic cognitive control. *Curr. Opin. Behav. Sci.* **4**, 152–159 (2015).
46. L. L. Jannasch, J. Grüb, A. Nieder, Shared cognitive biases influence numerical judgments in macaques and crows. *Proc. Natl. Acad. Sci. U.S.A.* **122**, e2512219122 (2025).
47. K. Merten, A. Nieder, Compressed scaling of abstract numerosity representations in adult humans and monkeys. *J. Cogn. Neurosci.* **21**, 333–346 (2009).
48. T. Machts, J. Grüb, A. Nieder, Neuronal encoding of recognition memory for numerical quantities in macaque intraparietal and prefrontal cortices. *Prog. Neurobiol.* **251**, 102794 (2025).
49. A. Nieder, The calculating brain. *Physiol. Rev.* **105**, 267–314 (2025).
50. A. Nieder, D. J. Freedman, E. K. Miller, Representation of the quantity of visual items in the primate prefrontal cortex. *Science* **297**, 1708–1711 (2002).
51. P. Viswanathan, A. Nieder, Spatial neuronal integration supports a global representation of visual numerosity in primate association cortices. *J. Cogn. Neurosci.* **32**, 1184–1197 (2020).
52. S. N. Jacob, T. Ott, A. Nieder, Dopamine regulates two classes of primate prefrontal neurons that represent sensory signals. *J. Neurosci.* **33**, 13724–13734 (2013).
53. T. Ott, A. M. Stein, A. Nieder, Dopamine receptor activation regulates reward expectancy signals during cognitive control in primate prefrontal neurons. *Nat. Commun.* **14**, 7537 (2023).
54. S. E. Cavanagh, J. P. Towers, J. D. Wallis, L. T. Hunt, S. W. Kennerley, Reconciling persistent and dynamic hypotheses of working memory coding in prefrontal cortex. *Nat. Commun.* **9**, 3498 (2018).
55. E. M. Meyers, Dynamic population coding and its relationship to working memory. *J. Neurophysiol.* **120**, 2260–2268 (2018).
56. J. P. Stroud, J. Duncan, M. Lengyel, The computational foundations of dynamic coding in working memory. *Trends Cogn. Sci.* **28**, 614–627 (2024).
57. C. E. Curtis, M. D'Esposito, Persistent activity in the prefrontal cortex during working memory. *Trends Cogn. Sci.* **7**, 415–423 (2003).
58. M. R. Riley, C. Constantinidis, Role of prefrontal persistent activity in working memory. *Front. Syst. Neurosci.* **9**, 181 (2015).
59. J.-R. King, S. Dehaene, Characterizing the dynamics of mental representations: The temporal generalization method. *Trends Cogn. Sci.* **18**, 203–210 (2014).
60. T. Ott, S. Westendorff, A. Nieder, Dopamine receptors influence internally generated oscillations during rule processing in primate prefrontal cortex. *J. Cogn. Neurosci.* **30**, 770–784 (2018).
61. R. Cools, A. F. T. Arnsten, Neuromodulation of prefrontal cortex cognitive function in primates: The powerful roles of monoamines and acetylcholine. *Neuropsychopharmacology* **47**, 309–328 (2022).
62. P. R. Corlett, K. M. Fraser, 20 years of aberrant salience in psychosis: What have we learned? *Am. J. Psychiatry* **182**, 819–829 (2025).
63. A. A. Grace, Dysregulation of the dopamine system in the pathophysiology of schizophrenia and depression. *Nat. Rev. Neurosci.* **17**, 524–532 (2016).
64. O. D. Howes, S. Kapur, The dopamine hypothesis of schizophrenia: Version III–the final common pathway. *Schizophr. Bull.* **35**, 549–562 (2009).
65. R. A. McCutcheon, A. Abi-Dargham, O. D. Howes, Schizophrenia, dopamine and the striatum: From biology to symptoms. *Trends Neurosci.* **42**, 205–220 (2019).
66. M. K. P. Joyce *et al.*, Higher dopamine D1 receptor expression in prefrontal parvalbumin neurons underlies higher distractibility in marmosets versus macaques. *Commun. Biol.* **8**, 974 (2025).
67. A. Thiele, L. S. Delicato, M. J. Roberts, M. A. Gieselmann, A novel electrode-pipette design for simultaneous recording of extracellular spikes and iontophoretic drug application in awake behaving monkeys. *J. Neurosci. Methods* **158**, 207–211 (2006).
68. P. Seeman, H. H. Van Tol, Dopamine receptor pharmacology. *Trends Pharmacol. Sci.* **15**, 264–270 (1994).
69. P. H. Andersen, J. A. Jansen, Dopamine receptor agonists: Selectivity and dopamine D1 receptor efficacy. *Eur. J. Pharmacol.* **188**, 335–347 (1990).
70. B. Levant, D. E. Grigoriadis, E. B. DeSouza, Characterization of [3H]quinpirole binding to D2-like dopamine receptors in rat brain. *J. Pharmacol. Exp. Ther.* **262**, 929–935 (1992).
71. M. Wang, S. Vijayraghavan, P. S. Goldman-Rakic, Selective D2 receptor actions on the functional circuitry of working memory. *Science* **303**, 853–856 (2004).
72. D. M. Green, J. A. Swets, *Signal Detection Theory and Psychophysics* (John Wiley, 1966).
73. A. J. Parker, W. T. Newsome, Sense and the single neuron: Probing the physiology of perception. *Annu. Rev. Neurosci.* **21**, 227–277 (1998).
74. E. Maris, R. Oostenveld, Nonparametric statistical testing of EEG- and MEG-data. *J. Neurosci. Methods* **164**, 177–190 (2007).
75. E. F. Kutter, Dopamine-D1-and-D2-Receptors-Differentially-Control-Abstract-Decision-Codes-in-Primate-PFC. GitHub. https://github.com/EstherKutter/Dopamine-D1-and-D2-Receptors-Differentially-Control-Abstract-Decision-Codes-in-Primate-PFC. Deposited 1 January 2026.